A Microcomputer-based GNSS Scintillation Monitor using Low-Cost Receiver

Manuel Allan Orongan[1,2], *Miemarc John* Deleña[1], *Ernest* Macalalad[2,*], *Sejera* Marloun[1], and *Tung Yuan* Hsiao[3]

[1] School of Electrical, Electronics, and Computer Engineering, Mapúa University, 658 Muralla St., Intramuros, Manila 1002, Philippines

[2] Department of Physics, Mapúa University, 658 Muralla St., Intramuros, Manila 1002, Philippines
[3] National Tsing Hua University, No. 101, Section 2, Guangfu Rd, East District, Hsinchu City, Taiwan

Abstract. We improve upon previous low-cost radio scintillation monitor designs by implementing onboard processing and display capabilities to produce a more comprehensive device. The proposed design uses a U-blox EVK-6T's GPS receiver, providing data updates at a rate of 1Hz, and a Raspberry Pi 4. The RPi calculates the S_{4c} index with both a three-minute and a five-minute duration, then saves all the raw data and S_{4c} values onto a locally stored CSV file. The proposed design has been successfully implemented, having been able to log all raw and calculated data and display the three-minute and five-minute S_{4c} values on a plot with a temporal range from 00 UT to 24 UT. In addition to these features, we successfully validate the accuracy of our low-cost radio scintillation monitor by finding a high correlation between its *C/No* output to that of a high-rate receiver when performing simultaneous measurements from the same receiving antenna. The S_{4c} values calculated from these *C/No* measurements also proved to be accurate as they demonstrated moderate correlation on non-scintillated days and high correlation on scintillated days.

1 Introduction

The ionosphere, an Earth's atmospheric layer containing charged particles, spans from about 60 to 1000 kilometers above the Earth's surface. Since the early era of radio communications, scientists and engineers have been intrigued by the study and comprehension of the ionosphere. They observed that radio signals could be prolonged by bouncing them off the ionosphere, a phenomenon called skywave propagation. Understanding the ionosphere has become essential with the introduction of artificial satellites since these satellites depend on signals passing through the ionosphere for communication with terrestrial stations [1].

Irregularities in the ionosphere can also form, especially during high solar activity, equinoxes and post-sunset hours. These may cause sudden changes in the amplitude and phase of radio frequencies passing through the ionosphere called scintillation [2, 3]. The S_4 index can be used to measure scintillation and is defined as the normalized standard deviation of the signal intensity I at a certain transmitting frequency over a given calculation interval [4]:

$$S_4 = \sqrt{\frac{\langle I^2 \rangle - \langle I \rangle^2}{\langle I \rangle^2}} \quad (1)$$

The severity of amplitude scintillations can be classified based on the S_4 index value: an S_4 index of 0.17 up to 0.3 indicates weak scintillation, values between 0.3 and 0.5 correspond to moderate scintillation and values greater than 0.5 indicate strong scintillation [5]. This phenomenon can impact the accuracy of GPS/GNSS positioning and, in general, disrupt satellite communications. Specifically, amplitude scintillation can affect the signal-to-noise ratio of the GPS receiver, leading to losses of lock and frequent cycle slips. Loss of lock occurs when the GNSS receiver can no longer accurately track the signal. In this state, navigation messages cannot be decoded, resulting in fewer visible satellites for positioning, while a cycle slip occurs when a receiver loses phase lock on a satellite's signal [6-9]. Consequently, the loss of lock and frequent cycle slips reduce the available GNSS satellites, ultimately degrading GNSS receiver performance and increasing positioning errors, especially in challenging environments where satellite visibility is obstructed. Therefore, it is important to detect and monitor these irregularities by tracking affected signals passing through the ionosphere to ensure the reliable operation of satellite communication technology.

Recognizing the necessity for more advanced ionospheric monitoring solutions, Rodrigues and Moraes took significant steps forward in their research. In 2019, they developed a low-cost ionospheric monitor named ScintPi. This monitor can measure L1 signals at a rate of up to 10 hertz. While the first iteration of ScintPi offered a low-cost solution for ionospheric monitoring, its signal-to-noise ratio (SNR) maxed out at 52 dB [10]. In 2022, ScintPi 2.0 and 3.0 addressed

* Corresponding author: epmacalalad@mapua.edu.ph

this limitation. ScintPi 2.0 expanded the SNR range, while ScintPi 3.0's dual-frequency receiver enabled the calculation of Total Electron Content (TEC) [11]. However, these low-cost iterations of ionospheric scintillation monitors do not have built-in processing capabilities or a way to show the results without using an additional device.

Taking inspiration from the ScintPi architecture, we design our own scintillation monitor but include real-time calculation and display capabilities of a proxy of the S_4 index, which we will be denoting as the S_{4c} index. This paper aims to study the feasibility of using this design with a low-cost single-frequency GNSS receiver to estimate L-band ionospheric scintillation through the provided carrier-to-noise density ratio (*C/No*) of the L1 band provided by a low-cost GPS receiver and demonstrate the real-time calculation and display capabilities of the S_{4c} index. The results are compared to a high-grade GNSS receiver.

2 Methodology

2.1 Scintillation index calculation

Proxy S_4 indices have been proposed by other studies to utilize off-the-shelf GNSS receivers for scintillation studies [4, 12]. In this study, instead of using the S_4 index, which relies on the knowledge of the signal intensity, we use its approximation, the S_{4c} index, which uses *C/No* as a crucial factor in its calculation as *C/No* is readily available through the NMEA-018 messages outputted by most low-cost off-the-shelf GNSS receivers. A study by Luo et al. found a strong correlation of over 0.9 between S_4 and S_{4c} [4], indicating the reliability of S_{4c} as an alternative scintillation index. To calculate S_{4c}, the conversion of the *C/No* ratio to the signal-to-noise density ratio (*S/No*) is necessary:

$$S/No = 10^{\frac{C/No}{10}} \tag{2}$$

After obtaining the *S/No*, assuming that the noise density remains approximately constant throughout the given trend duration of 60 seconds, the detrended signal intensity can be estimated by dividing the *S/No* value at the current epoch by the average *S/No* over a 60-second duration. This estimation is denoted as $I_{C/No}$ is given by

$$I_{C/No} = \frac{S/No}{\langle S/No \rangle} \tag{3}$$

Lastly, S_{4c} can be computed similarly to S_4, utilizing $I_{C/No}$ instead of I, as follows

$$S_{4c} = \sqrt{\frac{\langle I_{C/No}^2 \rangle - \langle I_{C/No} \rangle^2}{\langle I_{C/No} \rangle^2}} \tag{4}$$

2.2 Experimental setup

As shown in Figure 1, we used a Haxron GPS500 survey antenna, under a clear sky view connected through a signal splitter to a u-blox EVK-6T GPS receiver with our microcomputer-based monitoring system and a dual-frequency, high-grade GNSS receiver, specifically the Trimble BD990 GNSS Receiver, which was used for data verification. The EVK-6T is connected to a Raspberry Pi 4 (RPi) which shows its output on a graphical user interface (GUI) displayed on a monitor. The system was set up at Mapua University's Intramuros campus in Manila, Philippines with coordinates 14.5907°N and 120.9784E°. Table 1 shows a brief summary of the specifications of the EVK-6T and BD990 to better understand the differences between the two systems.

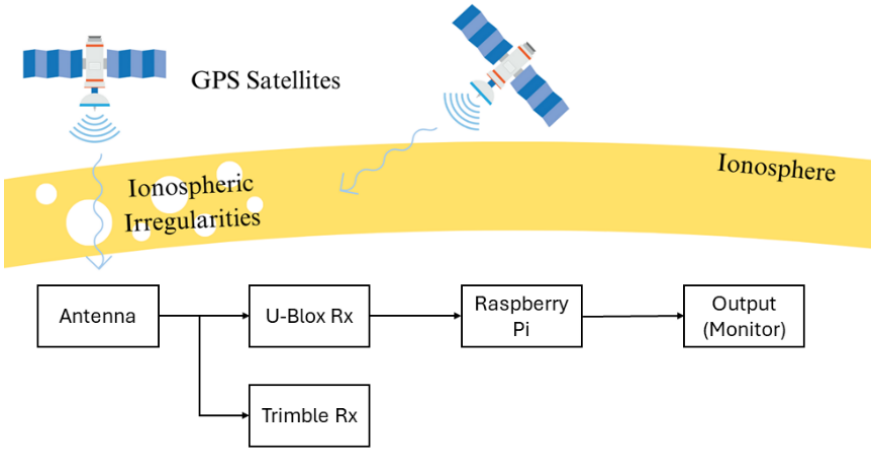

Fig 1. Experimental Setup

Table 1. Relevant specifications of the u-blox EVK-6T GPS receiver and the Trimble BD990 GNSS Receiver

Receiver Specifications	Maximum Sampling Rate (Hz)	C/No Resolution (dB-Hz)	Frequency bands	Receiver Type
EVK-6T	10	1	L1	Single-constellation (GPS)
BD990	50	0.1	L1, L2, L5	Multi-constellation (GPS, GLONASS, BeiDou, and Galileo)

2.3 System process flow

The system process flow describing how the radio signals from GNSS is translated to the desired output is shown in Figure 2. Here, radio signals received by the GPS antenna were translated into NMEA-0183 messages by the EVK-6T GPS receiver. These NMEA messages were then relayed to the RPi, where they were parsed, and relevant data were logged. Included in the logged raw data were the time of observation in UT, the PRN number of the received radio signal's originating satellite, that satellite's elevation and azimuth, and the C/No value of the received signal. After logging the raw data, the system then began to calculate the S_{4c} index for a three-minute and a five-minute calculation interval. After performing these calculations, the computed values were logged onto the same CSV file as the raw data. Simultaneously the system waited every 10 minutes to plot the S_{4c} values and update the plot shown on the monitor. To avoid data that is likely to be highly influenced by multipath effects, only satellites with elevation >30° were plotted onto the monitor. Similarly, only the data from satellites with elevation >30° were considered for subsequent data analysis.

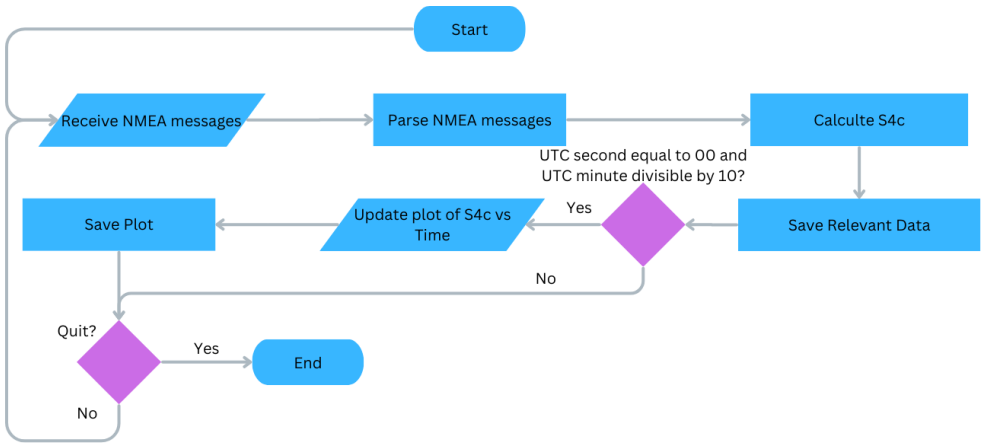

Fig 2. System process flow graph

3 Results and Discussion

As an example of observations without scintillation, we show the data from GPS 26, 27, 28, and 31 on July 12, 2024, as seen in Figure 3. On the other hand, we also show data with moderate scintillation event from July 13, 2024, from the same set of satellites in Figure 4. Both plots show the S_{4c} data derived from the receivers EVK-6T in red and BD990 in blue and the satellite elevation in black. The time of observation is shown on the horizontal axis from 12 UT (8:00 PM local time) to 20 UT (4:00 AM local time).

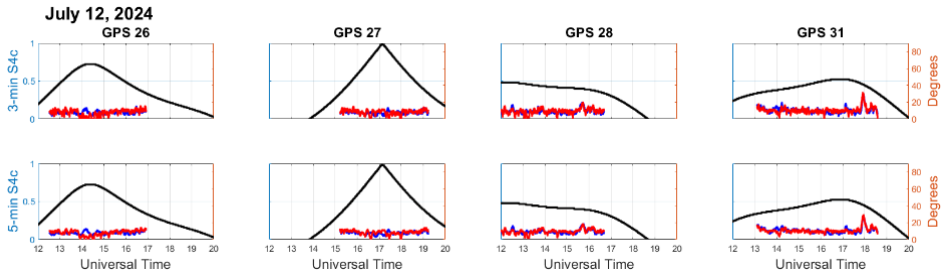

Fig 3. Sample 3-minute (top row) and 5-minute (bottom row) S4c outputs from a day without scintillation with satellite elevation (black) from the EVK-6T (red) and BD990 (blue) receivers for GPS 26, 27, 28, and 31 (1st to 4th columns, respectively) on July 12, 2024.

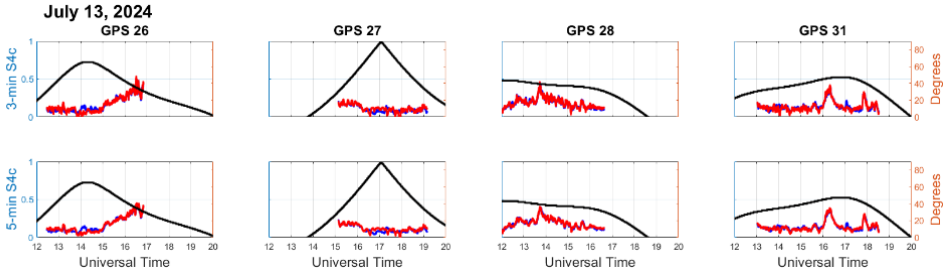

Fig 4. Sample 3-minute (top row) and 5-minute (bottom row) S_{4c} indices from a day moderate scintillation (July 13), with satellite elevation (black) from the EVK-6T (red) and BD990 (blue) receivers for GPS 26, 27, 28, and 31 on July 13, 2024.

On a quiet, non-scintillated day, the S_{4c} index remains mostly below 0.2, except for brief isolated spikes such as the one seen from GPS 31 at around 18 UT that we cannot confidently claim are due to ionospheric effects. We also see that the S_{4c} index remains unaffected by the satellite elevation, indicating that the elevation mask is sufficiently high to eliminate multipath effects. Otherwise, we would expect an increase in the S_{4c} index at lower elevation angles as multipath would cause interference in the signal [13]. In contrast, the data from the scintillated day shows characteristic signs of signal fluctuations. This may probably be caused by equatorial plasma bubbles (EPBs) when they are formed during post-sunset hours. This may affect GNSS signals throughout the night, causing long durations of heightened S_{4c} [5, 14]. Interestingly, we also see the same isolated spike in the S_{4c} index of GPS 31 at around 18 UT. Further study of this occurrence may be required.

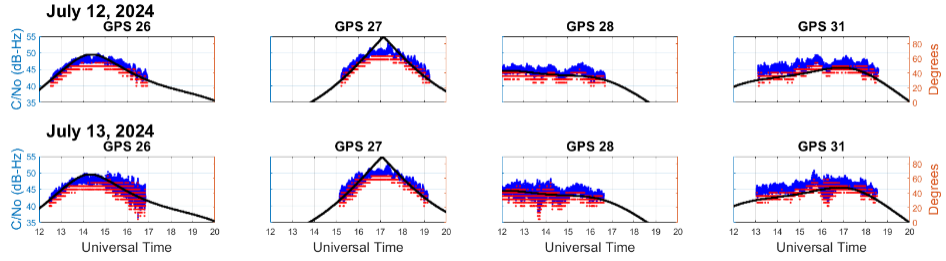

Fig 5. Sample *C/No* outputs from a day without scintillation (July 12, top row) and with scintillation (July 13, bottom row) for GPS 26, 27, 28, and 31 with satellite elevations (black) from the EVK-6T (red) and BD990 (blue) receivers.

C/No data received from the receivers EVK-6T and BD990, as well as the satellite elevation on July 12 and 13, 2024, from the hours of 18 UT to 20 UT, are shown in Figure 5. From both the quiet and scintillated days, we see that the *C/No* value generally increases with higher elevation. This is expected as a higher elevation means a shorter path between the satellite and receiver, decreasing free-space loss and making the signal less susceptible to other sources of loss [13]. Comparing the two, we see there is a significantly greater spread in the *C/No* values measured on the day with scintillation,

which is expected from a heightened S_{4c} index as we had earlier described amplitude scintillation to be rapid fluctuations in signal amplitude which is closely correlated with the *C/No*. It is important to note that the horizontal line pattern seen with the data from the EVK-6T is due to its 1 dB-Hz *C/No* resolution, making it output only integer values of the *C/No*. We also see an underestimation of the *C/No* by our system compared to the Trimble BD990 receiver, which we will later quantify with a linear correlational analysis between the two systems. The underestimation is likely due to differences in the receiver type and quality, as the noise observed can have significant variations between different receivers, causing differences in the reported *C/No* measurements [15].

Figure 6 shows the linear correlation between the *C/No* values from the two systems for the combined quiet data from July 12 and 15, 2024, and the combined days with moderate scintillation, July 13 and 14, 2024. Each plot also shows the data's root mean squared error (RMSE), the correlation coefficient (r), and the equation of the best-fit line along with the best-fit line in orange and the 1:1 as a black dashed line. By comparing the best-fit line with the 1:1 line, we confirm that our system generally underestimates the *C/No* value yet remains highly correlated with the measurements made by the BD990 at a correlation coefficient of 0.9394 with an RMSE of 1.654 dB-Hz for the quiet days and a correlation coefficient of 0.9277 with an RMSE of 1.682 dB-Hz for the days with scintillation. Both correlations have a slope of about 0.92 and y-intercept of about 2. Though not significantly, we see a higher correlation and a lower RMSE on days without scintillation. Similar to the sample of the *C/No* values, the horizontal line pattern is a byproduct of the 1 dB-Hz *C/No* resolution of the EVK-6T GPS receiver.

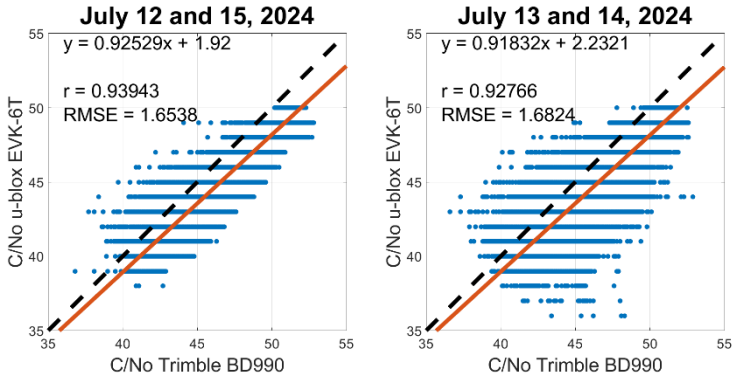

Fig 6. Linear correlation of *C/No* outputs on July 12 and 15 (left), and July 13 and 14 (right) from the EVK-6T and BD990 receivers. Both plots are shown with their best-fit line, correlation coefficient r and RMSE.

Next, we consider the correlation between the three-minute and five-minute S_{4c} values computed from the two systems for the quiet days and scintillated days in Figure 7. Again, the RMSE, correlation coefficient, and equation of the best-fit line are shown on each plot, with the best-fit line in orange and the 1:1 line as a black dashed line. Having slopes that range from 0.7 to 0.88, it shows that during scintillation events, the system estimates S_{4c} relatively lower than BD990. We see a moderate correlation of 0.6388 and 0.6889 on the quiet days for the three-minute and five-minute S_{4c} indices, respectively. In contrast, we see a significantly higher correlation of 0.8181 and 0.8569 on the days with scintillation for their three-minute and five-minute S_{4c} indices, respectively. We also see that the best-fit line matches the 1:1 line more closely on days with scintillation than on days without scintillation.

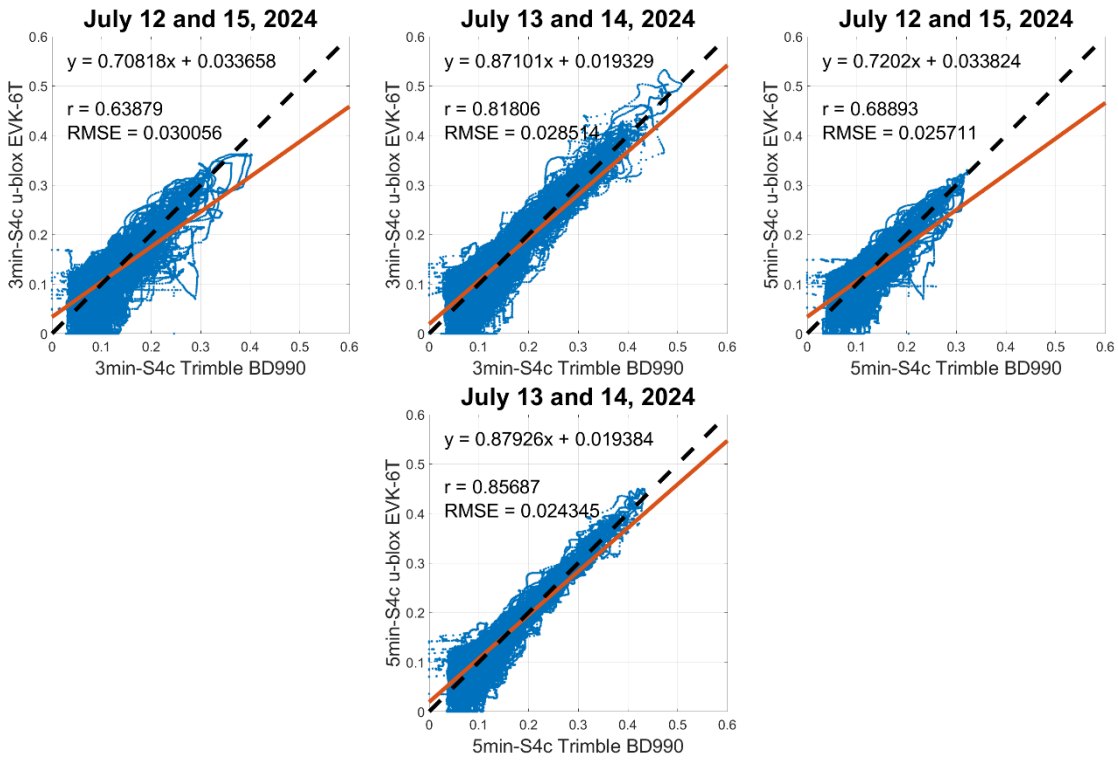

Fig 7. Linear correlation of 3-minute (top row) and 5-minute (bottom row) S_{4c} outputs of the EVK-6T and BD990 receivers on July 12 and 15 (left column), and July 13 and 14 (right column).

The difference in correlation coefficient and best-fit line is likely due to our system's 1 dB-Hz *C/No* resolution, which makes low S4c measurements less precise. This same issue of increased error in the scintillation index during no significant scintillation was also experienced by Rodrigues and Morales when making their ScintPi sensor, which they also claimed to be due to low resolution [10].

4 Summary and Recommendations

We present the results and discussion of our proposed system for real-time monitoring of ionospheric scintillation through amplitude scintillation. The system utilizes a u-blox EVK-6T GPS receiver and a Raspberry Pi 4.

We were able to show the prototype measuring real-time data of the S4c index and displaying them onto our GUI by deploying it at Mapua University Intramuros Campus in Manila, Philippines from July 12 to 15, 2024. Simultaneously, observations were conducted to test the system's ability to detect scintillation activities. A comparison with a high-rate GNSS receiver (Trimble BD990) confirmed the validity of our system. The comparison yielded positive results, showing a strong correlation between the *C/No* values with or without scintillation, strong correlation for S4c indices on days with scintillation but only a moderate correlation for S4c indices when there was no significant scintillation detected.

As the system currently only measures amplitude scintillation to observe ionospheric irregularities, it is crucial to enhance its analytical capabilities. We recommend incorporating real-time monitoring features for both the phase scintillation index σ_φ and Total Electron Content (TEC). Real-time monitoring of σ_φ, which measures phase scintillation, will provide another avenue for insights into variations in signal quality and stability, thereby improving the system's ability to track and analyze the impact of scintillation on signal integrity. Additionally, integrating real-time TEC monitoring will enable the system to assess fluctuations in the ionosphere's electron density, which is crucial for understanding and mitigating ionospheric disturbances affecting signal propagation and accuracy. By adding these features, the system will provide more comprehensive and timely data, leading to more robust analysis and effective solutions.

References

1. C. Huang and G. Lu, Space Physics and Aeronomy, Ionosphere Dynamics and Applications. (John Wiley & Sons, 2021)
2. E.P. Macalalad, Solar Activity and Temporal Dependence of Rate of Change of Ionospheric Total Electron Content in Low-Latitude Region, in Proceedings of 2023 IEEE International Conference on Aerospace Electronics and Remote Sensing Technology (ICARES), Bali, Indonesia, October 26-27 (2023). https://doi.org/10.1109/ICARES60489.2023.10329904

3. K. E. S. Juadines, E. P. Macalalad, and M. M. Mendoza, Observation of Low-Latitude Ionospheric Irregularities using Rate of Change of Total Electron Content over the Philippine Sector, in Proceedings 2019 6th international Conference on Space Science and Communication (IconSpace), Johor Bahru, Malaysia, July 28-30 (2019). https://doi.org/10.1109/IconSpace.2019.8905976
4. X. Luo, S. Gu, Y. Lou, L. Cai, and Z. Liu, Amplitude scintillation index derived from C/N0 measurements released by common geodetic GNSS receivers operating at 1 Hz, J Geod, **94**, 2 (2020). https://doi.org/10.1007/s00190-020-01359-7
5. R. K. Vankadara, P. Jamjareegulgarn, G. K. Seemala, M. I. H. Haque, and S. K. Panda, Trailing Equatorial Plasma Bubble Occurrences at a Low-Latitude Location through Multi-GNSS Slant TEC Depletions during the Strong Geomagnetic Storms in the Ascending Phase of the 25th Solar Cycle, Remote Sensing, **15**, 20, 4944 (2023). https://doi.org/10.3390/rs15204944
6. G. Sivavaraprasad, R. S. Padmaja, and D. V. Ratnam, Mitigation of ionospheric scintillation effects on GNSS signals using variational mode decomposition, IEEE Geoscience and Remote Sensing Letters, **14**, 3, 389–393 (2017). https://doi.org/10.1109/lgrs.2016.2644723
7. M. Van De Kamp, P. S. Cannon, and M. Terkildsen, Effect of the ionosphere on defocusing of space-based radars, Radio Science, **44**, 1 (2009). https://doi.org/10.1029/2007rs003808
8. Y. Liu, L. Fu, J. Wang, and C. Zhang, Study of GNSS Loss of Lock Characteristics under Ionosphere Scintillation with GNSS Data at Weipa (Australia) During Solar Maximum Phase, Sensors, **17**, 10, 2205 (2017). https://doi.org/10.3390/s17102205
9. Cycle Slip | GEOG 862: GPS and GNSS for Geospatial Professionals. Available online: https://www.e-education.psu.edu/geog862/node/1728
10. F. S. Rodrigues and A. O. Moraes, SCINTPI: a Low-Cost, Easy-to-Build GPS ionospheric scintillation monitor for DASI studies of space weather, education, and citizen science initiatives, Earth and Space Science, **6**, 8, 1547–1560 (2019). https://doi.org/10.1029/2019ea000588
11. J. G. Socola and F. S. Rodrigues, ScintPi 2.0 and 3.0: low-cost GNSS-based monitors of ionospheric scintillation and total electron content, Earth Planets and Space, **74**, 1 (2022). https://doi.org/10.1186/s40623-022-01743-x
12. K. E. Juadines, A. Ballado, E. Macalalad, and M. Mendoza, Development of a MATLAB Web-based Application for Calculating Ionospheric Scintillation Proxy Indexes (S4p-1 and S4p-2) and the Rate of Total Electron Content Index (RoTI), in Proceedings 2021 IEEE World AI IoT Congress (AIIoT), May 10-13 (2021). http://doi.org/10.1109/AIIoT52608.2021.9454235
13. N. I. Muhammad, M. Y. Abdullahi, and Y. S. Abu, A review of the effect of low elevation angles on the propagation for satellite communication link, FUDMA Journal of Sciences, **7**, 1(2023). http://doi.org/10.33003/fjs-2023-0701-1270
14. T. Thanakulketsarat, P. Supnithi, L. M. M. Myint, K. Hozumi, and M. Nishioka, Classification of the equatorial plasma bubbles using convolutional neural network and support vector machine techniques, Earth Planets and Space, **75**, 1 (2023). https://doi.org/10.1186/s40623-023-01903-7
15. H. Zhang, S. Ji, Z. Wang, and W. Chen, Detailed assessment of GNSS observation noise based using zero baseline data, Advances in Space Research, **62**, 9 (2018). https://doi.org/10.1016/j.asr.2018.07.023